Top Curr Chem (Z) (2017) 375:90
https://doi.org/10.1007/s41061-017-0178-8

REVIEW

Recent Developments in Single-Walled Carbon Nanotube Thin Films Fabricated by Dry Floating Catalyst Chemical Vapor Deposition

Qiang Zhang[1] · Nan Wei[1] · Patrik Laiho[1] · Esko I. Kauppinen[1]

Received: 14 September 2017 / Accepted: 13 November 2017 / Published online: 27 November 2017

Abstract Transparent conducting films (TCFs) are critical components of many optoelectronic devices that pervade modern technology. Due to their excellent optoelectronic properties and flexibility, single-walled carbon nanotube (SWNT) films are regarded as an important alternative to doped metal oxides or brittle and expensive ceramic materials. Compared with liquid-phase processing, the dry floating catalyst chemical vapor deposition (FCCVD) method without dispersion of carbon nanotubes (CNTs) in solution is more direct and simpler. By overcoming the tradeoff between CNT length and solubility during film fabrication, the dry FCCVD method enables production of films that contain longer CNTs and offer excellent optoelectronic properties. This review focuses on fabrication of SWNT films using the dry FCCVD method, covering SWNT synthesis, thin-film fabrication and performance regulation, the morphology of SWNTs and bundles, transparency and conductivity characteristics, random bundle films, patterned films, individual CNT networks, and various applications, especially as TCFs in touch displays. Films based on SWNTs produced by the dry FCCVD method are already commercially available for application in touch display devices. Further research on the dry FCCVD method could advance development of not only industrial applications of CNTs but also the fundamental science of related nanostructured materials and nanodevices.

This article is part of the Topical Collection"Single-Walled Carbon Nanotubes: Preparation, Property andApplication"; edited by Yan Li, Shigeo Maruyama.

✉ Qiang Zhang
qiang.zhang@aalto.fi

[1] Department of Applied Physics, Aalto University School of Science, P.O. Box 15100, 00076 Aalto, Finland

Keywords Single-walled carbon nanotubes · Dry floating catalyst chemical vapor deposition · Transparent conducting film · Touch displays

1 Introduction

Since their discovery, carbon nanotubes (CNTs) have been the subject of intensive research [1–3]. CNTs can be thought of as graphene sheets rolled up in certain directions, designated by pairs of integers, existing as both single-walled nanotubes (SWNTs) and multiwalled nanotubes (MWNTs) [4, 5]. Compared with MWNTs, SWNTs have been shown to exhibit very distinct properties, providing greater potential for use of this outstanding structural material in nano- and macroscale applications [1, 6]. Depending on their chirality and diameter, SWNTs can be either semiconducting, metallic, or semimetallic in nature [7]. Both experiments and theory have confirmed that CNTs possess excellent and unique characters, which originate from their molecular structure [7]; For example, SWNTs possess high conductivity (up to 4×10^5 S cm^{-1}) [8], excellent current-carrying capacity (up to 10^9 A cm^{-2}) [9], excellent charge-carrier mobility (up to 10^5 cm^2 V^{-1} s^{-1} at room temperature) [10], excellent thermal conductivity (up to 3500 W m^{-1} K^{-1}) [11], and excellent mechanical performance (Young's modulus in the range of 1–2 TPa) [12, 13].

Over recent decades, numerous academic and industrial groups have explored use of SWNTs in diverse potential applications [1, 14]. In particular, SWNTs with various types of architecture and different dimensions have been synthesized and investigated worldwide to fully utilize the excellent properties of individual SWNTs [15–18]. Thin films is an emerging research area, offering the advantage of statistical averaging for better reproducibility [14, 19–21]. The collective behavior of two-dimensional (2D) SWNT films can provide unique physical properties and enhanced device performance [22]. Their superior properties, including mechanical flexibility, optical transparency, unique electric properties, high surface area, etc., result in great potential for use of CNT films the applications in energy fields, electronic devices, displays, sensors, etc [19, 20]. However, some important challenges remain to be resolved: (1) controlled fabrication of SWNT films with good reproducibility, (2) utilization of the excellent properties of individual SWNTs at macroscopic level, and (3) prediction or exploration of new properties offered by macroscopic SWNT assemblies.

To date, several methods have been developed to fabricate CNT films. Specifically, two main types of process, i.e., liquid-phase and dry processing, have been used to assemble CNT films [19]. Liquid-phase processing involves deposition of tubes from surfactant solution or superacids to form CNT thin films, which is readily scalable. However, a practical challenge with such liquid-phase methods is that the low solubility and strong intertube interactions of SWNTs make it difficult to obtain submonolayer SWNT thin films with uniform, moderate to high coverage and without significant presence of bundles [23, 24]. Complete removal of residual surfactants and acids is also a difficult problem. Dry methods for fabrication of CNT

films mainly include three approaches: growth directly by on-substrate CVD, drawing from a vertically aligned CNT forest grown on a solid substrate, or deposition directly from a floating catalyst chemical vapor deposition (FCCVD) system. CNT networks can be grown directly on a substrate by CVD. The orientation, density, and even chiral distribution of the CNTs can be controlled by using selected and regulated catalysts on the substrate [25–27]. However, such on-substrate CVD normally requires multistep processing and has low yield. The aligned CNT films drawn from a CNT forest are anisotropic [28]. However, devices based on aligned CNT film components offer poor statistical reproducibility. SWNT films cannot be obtained from the CNT forest method. In addition, intricate treatment is needed to obtain MWNT films from a CNT forest for special applications; For example, laser trimming and metal deposition increase the transmittance and conductivity, respectively, when using MWNT films as transparent conductive films [29]. On the other hand, film fabrication by the FCCVD method is based on direct deposition of an SWNT aerosol synthesized by the FCCVD method [22, 30–32]. FCCVD is low-cost and readily scalable and offers good control over the morphology of the CNTs or bundles in the thin film, including their length, diameter, density, etc., which are critical parameters for film performance. In particular, films fabricated by the FCCVD method can contain individual SWNTs of theoretically unlimited length [33]. These characteristics will lead to many novel results and great improvements in CNT applications.

This review focuses on fabrication of films using the dry FCCVD method, as well as corresponding SWNT synthesis, thin-film fabrication and performance regulation, transparency and conductivity characteristics, random bundle films, patterned films, and individual CNT networks; in addition, various applications, especially as transparent conductive electrodes (TCEs), are highlighted. The final section concludes with some long-standing problems and identifies topics warranting further investigation in the near future.

2 CNT Synthesis Process and Mechanism

The research fields of CNT synthesis and CNT films are interdependent. Many key advances in CNT catalysts and synthesis lead immediately to new results in film fabrication, performance, and applications. There are three major methods of CNTs production: arc discharge, laser ablation, and chemical vapor deposition (CVD) [34]. Owing to its high yield and relatively mild synthesis conditions, CVD is the most common method used for CNT growth. However, most products synthesized by CVD are mainly powder like or supported on different substrates. FCCVD, as a special CVD method, has attracted tremendous attention. Since the catalyst particles and CNTs are suspended in gas phase as an aerosol throughout the entire CNT formation process, the FCCVD method is more flexible and controllable [29], not only being an effective approach to mass-produce CNTs of good quality [36] but also enabling direct synthesis of different SWNT architectures, such as continuous fibers [18, 37], transparent films [22, 31] ,and CNT sponges [38].

Many features of FCCVD can affect the morphology and properties of the resulting CNTs, with catalyst composition, catalyst size, carbon source, temperature, and gas-phase chemistry being the five principal parameters [39, 40]. The most effective catalysts for FCCVD are formed from pyrolysis of easily sublimed organometallic compounds, such as ferrocene, carbonyl iron, dimethoate, or metal nanoparticles generated using a hot-wire or spark system [35, 41, 42]. In 1998, Cheng et al. first applied the FCCVD method to synthesize SWNTs using ferrocene as catalyst [6, 43]. This result suggested that FCCVD is a potential method for high-yield production of CNTs. The catalyst size is slightly larger than the diameter of the resulting nucleated CNTs, a phenomenon also observed in on-substrate CVD and in situ growth in environmental transmission electron microscope [41]. Many excellent carbon sources for production of CNTs are known, including hydrocarbons and carbon monoxide (CO) [40]. Hydrocarbons thermally self-decompose into carbon clusters (C_xH_y), which are then absorbed by the catalyst. This process contributes to rapid and high-yield growth of CNTs [44]. However, high partial press of the hydrocarbon or temperature may result in production of surplus amorphous carbon [45]. CO as carbon source is significantly different from hydrocarbons; It decomposes only at the surface of the catalyst nanoparticles, liberating carbon atoms for CNT formation, since the disproportionation reaction $2CO(g) \leftrightarrow C(s) + CO_2(g)$ requires the presence of a catalyst surface [35, 36]. This reaction can greatly reduce byproduct generation. SWNT production based on CO disproportionation has been carried out at either high or atmospheric pressure (Fig. 1), and both methods are widely applied for commercial production of SWNTs and films. In 2001, Smalley's group [36] developed the high-pressure CO (HiPCO)

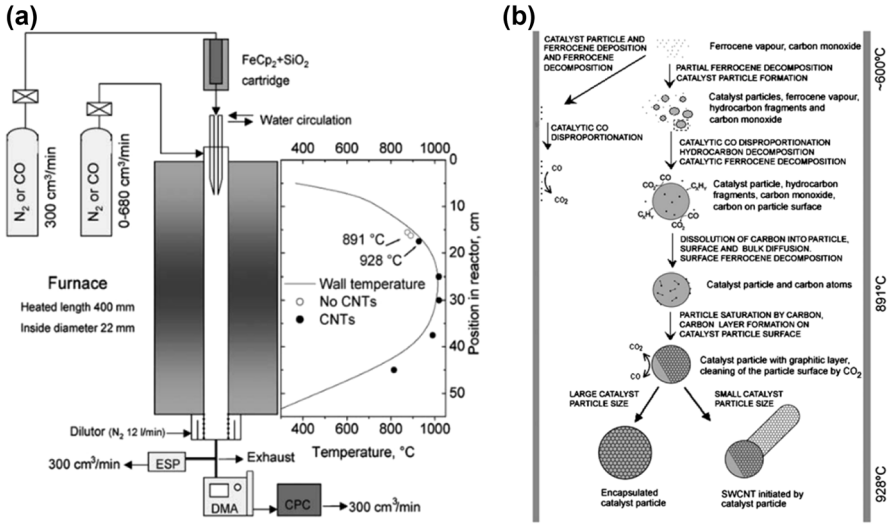

Fig. 1 High-quality SWCNTs synthesized with CO as carbon source at atmospheric pressure based on FCCVD [54]. Copyright 2006 Elsevier. **a** Schematic of experimental setup and wall temperature profile for FCCVD synthesis of SWCNTs with ferrocene as catalyst. Open circles indicate sampling locations where CNTs were not observed; solid circles indicate conditions for CNT sampling. **b** Schematic of SWCNT formation mechanism in $FeCp_2$–CO system at temperature of 1000 °C

approach to produce large quantities of SWNTs in presence of iron nanoparticles formed from decomposition of iron pentacarbonyl. More recently, He et al. [46] and Koziol et al. [40] examined the structural differences between tubes grown using CO, methane, ethanol, and toluene by electron diffraction methods. The optimal growth temperature appeared to range from 700 to 1200 °C, lying between the temperature for amorphous carbon formation and the graphitization temperature. Argon, helium, nitrogen, and hydrogen are commonly used as carrier gas for feedstock introduction and product carriage, although less research has been carried out on the difference between use of argon, helium, or nitrogen for CNT growth. It is reported that hydrogen can effectively suppress excessive decomposition of hydrocarbons and also reduce iron oxide during production of CNTs [47, 48]. In addition, hydrogen can etch amorphous carbon and CNTs. In 2014, Liu et al. reported production of 88% metallic SWNTs (m-SWNTs) when introducing H_2 as etchant to selectively etch semiconducting SWNTs (s-SWNTs) (Fig. 2) [49]. Based on the effect of tuning the growth parameters, it was proposed that small-diameter s-SWNTs and large-diameter m-SWNTs were first obtained, then introduction of hydrogen as etchant gas preferentially removed the smaller-diameter s-SWNTs. In the cited work, few-wavelength Raman was used to determine the fraction of metallic and semiconducting tubes. Due to the complexity of evaluation of such Raman spectra for assignment of CNT-type distributions, more accurate analysis methods are needed, e.g., electron diffraction, for determination of the metallic tube fraction [40, 50–52].

To obtain high-quality, high-yield SWNTs and films at atmospheric pressure, several crucial improvements have been made to the FCCVD method at Aalto University, including a well-designed FCCVD system and use of a CNT synthesis mechanism with CO as carbon source [35, 41, 53, 54]. As shown in Fig. 1a, the laminar reactor for SWNT production includes a water-cooled injector and a vertical furnace [35]. The injector probe reaches into the high-temperature zone of the vertical CVD reactor. Recirculation of the additional flow occurs only in the region close to the injector probe outlet. However, the flow containing the nanoparticles does not take part in the recirculation, and the total flow becomes fully developed and laminar as it moves towards the high-temperature zone of the furnace,

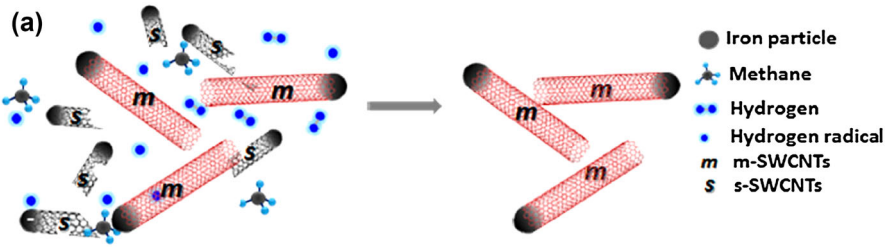

Fig. 2 Schematics proposing selective removal of small-diameter s-SWNTs from large-diameter m-SWNTs by hydrogen etching [49]. Copyright 2014 American Chemical Society

indicating laminar flow conditions for catalyst particle formation and SWNT growth. Use of this type of equipment can effectively reduce catalyst deposition on the reactor wall. The aerosol of catalyst or precursor, carbon source, and carrier gas are introduced through the injector probe into the high-temperature zone of the vertical CVD reactor. Floating CNTs and bundles can be directly and continuously obtained at the reactor end. The mechanism for SWNT formation in the $FeCp_2$–CO system is shown in Fig. 1b. Decomposition of $FeCp_2$ vapor results in catalyst particle formation and likely release of hydrocarbon fragments. Catalyst particles are formed by nucleation and continue to grow through collision processes. In addition, catalyst particle growth can continue as a result of ferrocene vapor decomposition on the particle surfaces. Depending on their size, the catalyst particles either nucleate growth of a SWNT or become inactive by growing too large (usually above 3 nm in diameter). In addition, through a series of CNT growth experiments, the growth window for temperature for the CO system was determined to be 891 to 928 °C [54]. In addition to high-quality SWNTs, a novel hybrid material, viz. nanobuds, in which fullerenes and SWNTs are combined into a single structure in which the fullerenes are covalently bonded onto the outer surface of the SWNTs, was invented at Aalto University. In 2007, based on the $FeCp_2$–CO system, carbon nanobuds (CNBs) were synthesized with increasing H_2O and CO_2 concentrations during the FCCVD process for synthesis of CNT [33, 55]. Due to their unique structure, CNBs possess advantageous properties compared with SWCNTs or fullerenes alone, including field-emission characteristics when in nonbonded configuration.

3 CNT Film Fabrication

Recently, the demand for TCFs has surged due to the expansion of the commercial market for optoelectronic devices such as liquid-crystal displays (LCDs), touch panels, photovoltaics, and organic light-emitting diodes (OLEDs) [56, 57]. In 2014, sales of TCFs in the LCD industry, which has led consumption for years, were approximately USD 1.5 billion [58] . In addition, the commercial market for TCFs in the solar industry is expected to exceed USD 16.3 billion by 2017 [59], and the market for TCFs in touch panels is anticipated to reach about USD 5 billion by 2019 [60].

Indium tin oxide (ITO) is the most widely used and current industry-standard transparent conductor material, offering excellent optoelectronic properties with low sheet resistance (R_s, from 10 to 100 Ω/sq) at high transmittance (> 85%) [57]. However, as a brittle ceramic, the limitations of its physical property have presented many challenges for development of flexible electronics [57, 61]. In addition, the high refractive index of ITO may result in images displayed on touch screens becoming washed out [61, 62]. Recently, various novel materials, including silver nanowires, metal mesh, graphene, and CNT films, have emerged as ITO replacement materials [56]. Owing to their low surface resistance due to the high conductivity of metal compared with ITO, silver nanowire films and metal mesh offer benefits for use in large-area touch displays [63]. However, there are also some severe problems with application of silver nanowires and metal meshes as TCFs,

such as performance stability and high ambient light reflectance [64]. The high cost and complex process of graphene synthesis seriously limit development of graphene for use as TCF [65]. Among these promising candidates, CNT TCFs exhibit great potential because of their high stretchability, mechanical flexibility, chemical stability, color neutrality, less haze, wider spectral range, etc. [56, 59, 66, 67].

4 2D Network Film

As mentioned above, FCCVD is a promising technique for SWNT film fabrication. It enables direct, single-step fabrication of clean, ready-to-use SWNT networks for use as high-performance TCFs. Currently, there are three main approaches for CNT film fabrication based on FCCVD, as shown in Fig. 3. The individual tubes or bundles produced by the FCCVD method are suspended in a carrier gas. Films can then be obtained by deposition of the CNTs or bundles onto a membrane filter [30, 31] or FCCVD chamber wall [22], or by direct transformation of the CNT aerosol into an aerogel [68]. The specific processes of film fabrication are discussed and compared below.

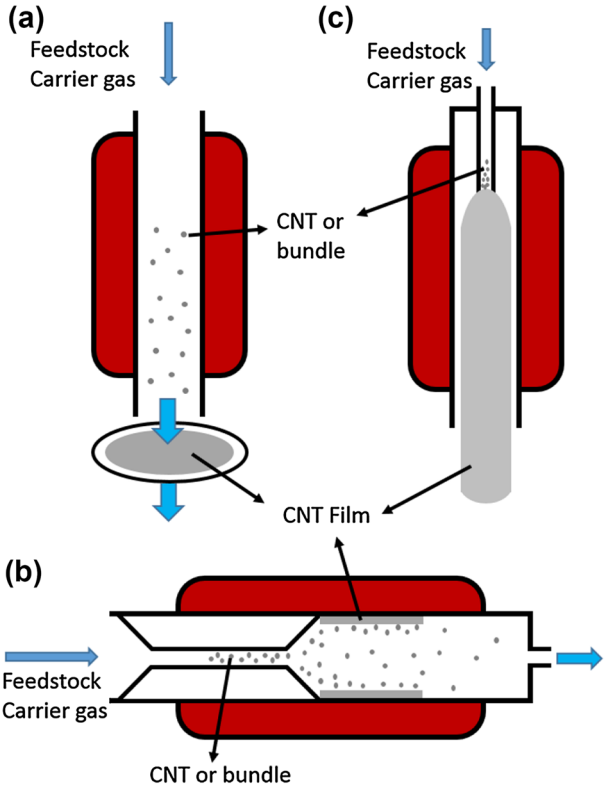

Fig. 3 Schematics of CNT film fabrication processes based on FCCVD, where CNTs and bundles are directly deposited onto a membrane filter (**a**) or FCCVD chamber wall (**b**), or **c** the CNT aerosol is transformed into an aerogel in the FCCVD reactor

CNT films can be prepared by dry deposition, combing the FCCVD method with an aerosol filtration system, as shown in Fig. 3a. The aerosol containing individual SWNTs and their small bundles is collected by a membrane filter at the outlet of the reactor to form a SWNT network. The sheet resistance and transmittance can be controlled by adjusting the network deposition time or reactor dimensions and conditions. In 2010, Kaskela et al. [31] integrated SWNTs collected on a nitrocellulose filter based on the laminar flow reactor with CO as carbon source and CO_2 as additive to enhance the catalyst particle activity (Fig. 4a). The micromorphology of the SWNT film was a continuous 2D network, as shown in Fig. 4b. The sheet resistance of the SWNT films with bundle length of 9.4 μm ranged from 80 to 100 Ω/sq at a transmission of $T = 90\%$ after HNO_3 doping. Since such SWNT

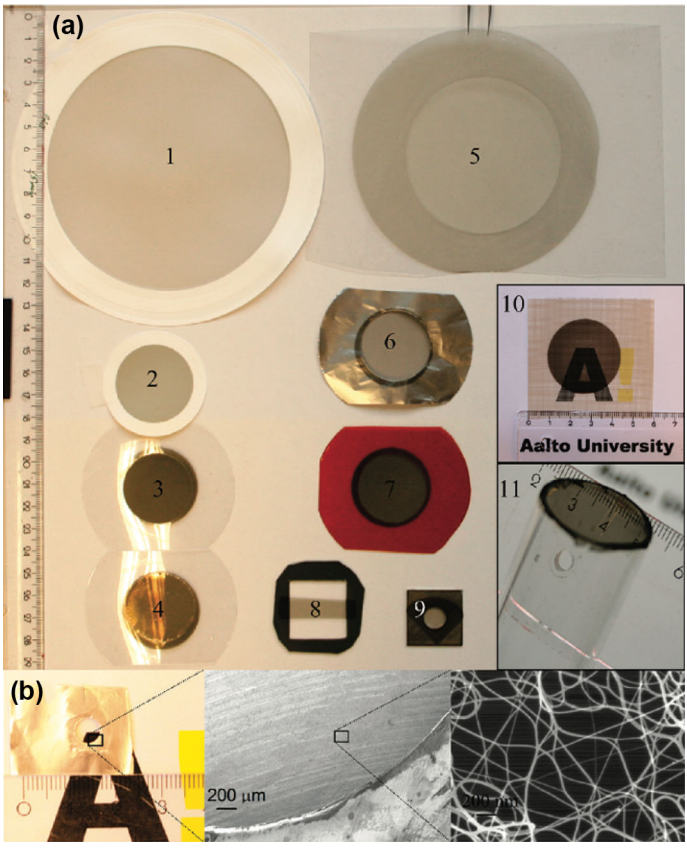

Fig. 4 Various SWNT films prepared by FCCVD [30] (Copyright 2011 American Chemical Society): **a** SWCNT films collected on nitrocellulose filters (*1*, *2*), pristine (*3*) and ethanol-densified (*4*) films suspended over polyethylene terephthalate (PET), freestanding films (FSFs) on PET (*5*), aluminum foil (*6*), and Kapton (*7*), a strip film suspended over a rectangular hole (*8*), and on cold-rolled steel (*9*). Insets show semi-freestanding film on polyetheretherketone substrate (*10*) and a film suspended over the open end of a glass tube (*11*). **b** Set of images showing submonolayer FSF suspended over 5-mm openings in aluminum foil

films are collected on low-adhesion filters, they can be easily transferred to practically any substrate, including flexible polymers, glass, quartz, and various metals, using a simple press. SWNT films with various thicknesses and sizes on different substrates are shown in Fig. 4. This simple film fabrication method is also called direct dry transfer [31]. In addition, the CNT aerosol can also be deposited onto the substrate surface downstream of the FCCVD system by using an electric field thermophoretic technique for thin-film manufacture [69].

The press transfer method is compatible with roll-to-roll fabrication methods, thus opening up further upscaling potential for industrialized production. In particular, Carbon NanoBud (CNB) film, a special SWNT film from Canatu, is already in commercial production [62]. Homogeneous and patterned CNB films can be manufactured on large size sheets by combining the CNB aerosol synthesis method with room-temperature deposition. The film conductivity of CNB film at given transparency has doubled approximately every 12 months since 2007. In 2013, CNB films with properties of 100 Ω/sq at 94% and 270 Ω/sq at 98% were commercially available. The facility allowed capacity of up to 500,000 m^2/month by Canatu. In addition, film performance of 100 Ω/sq at >95% has been demonstrated [62].

Ma et al. [22] directly prepared SWNT films with methane as carbon source, argon as carrier gas, $FeCp_2$ as catalyst, and sulfur as promoter in 2007. During their preparation process, the CNTs are deposited on the FCCVD chamber wall in the high-temperature zone, then grow continuously to form CNT films (Fig. 3b) that can be easily peeled off after growth. The thickness of such freestanding and homogeneous SWNT films, with area up to several tens of square centimeters, can be regulated from 100 nm to 1 μm (Fig. 5a, b, c). These SWNT films are composed of highly entangled bundles about 30 nm in diameter and from tens to hundreds of micrometers in length (Fig. 5d, e). The diameter of the nanotubes in the bundles is about 1–2 nm. The bundles in the films are firmly connected with each other, as they grow to forming a continuous, preferentially 2D network at high temperature (Fig. 5e). Due to these good and long interbundle connections, such directly synthesized films offer good electrical and mechanical properties, with electrical conductivity of 2000 S/cm and strength of 360 MPa. Figure 5 f, g shows transmittance spectra from the ultraviolet to mid-infrared and the sheet resistance of freestanding SWNT films of different thicknesses. For 100-nm-thick film with sheet resistance of 50 Ω/sq, which was the thinnest intact film that could be peeled off the wall of the quartz tube, the transmittance in the visible region of the spectrum was above 70%.

In addition, freestanding CNT films can also be fabricated by transformation of the CNT aerosol into an aerogel using a well-designed FCCVD system. In 2013, Zhou et al. [68] introduced a blown aerosol technique into the process of CNT synthesis by FCCVD for continuous CNT film production (Fig. 3c). With injection of the feedstock for CNT synthesis and the carrier gas, transparent tubular films with diameter of ~100 mm were continuously blown out from the outlet of the FCCVD system at speed of ~120 m/h. The surface resistance of the as-synthesized SWNT films was ~200 Ω/sq at transmission of $T = 90\%$, for the optimized conditions. In

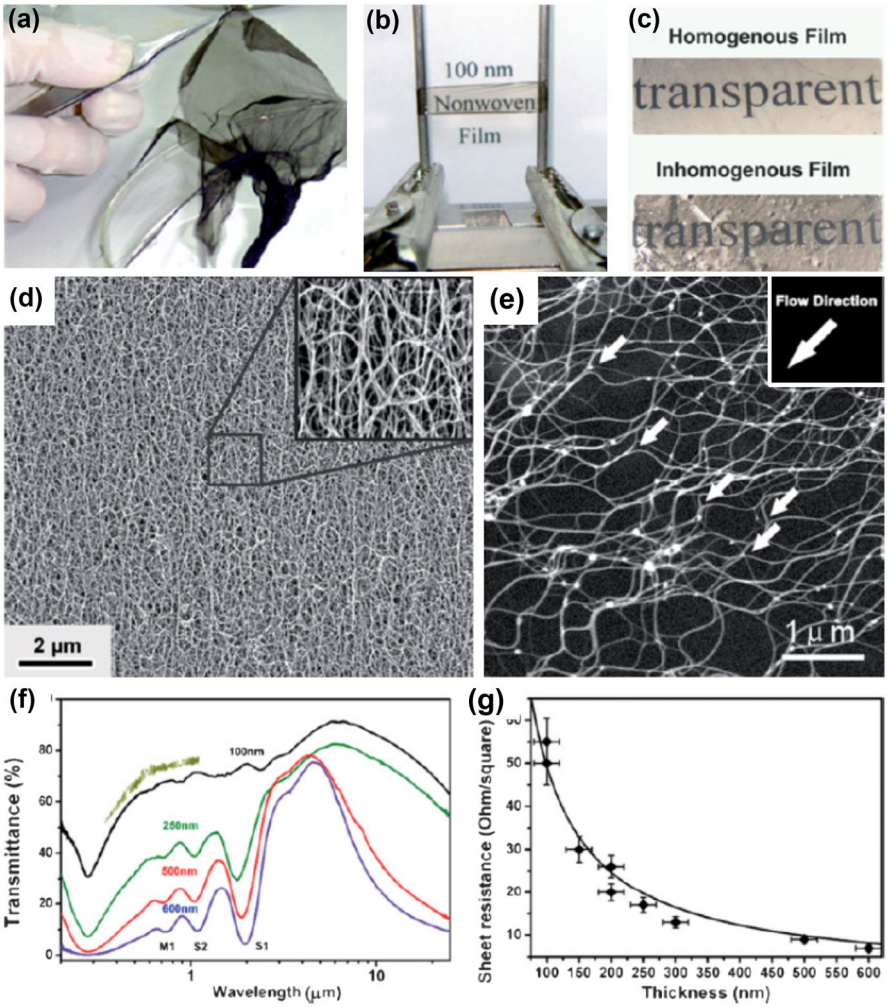

Fig. 5 **a** As-grown 250-nm-thick SWCNT nonwoven film. **b** Transparent 100-nm-thick film standing freely between metallic pillars. **c** 150-nm-thick homogeneous (upper) and inhomogeneous films. The importance of homogeneity is clear. **d** Large-scale scanning electron microscopy (SEM) image of 250-nm-thick film; inset shows higher magnification. **e** SEM image of SWCNT network in a single layer; white arrows indicate Y-type junctions and flow direction. **f** Transmittance spectra for as-grown films of different thicknesses. Numbers above curves indicate thickness, and the uppermost short curve corresponds to 100-nm-thick film on glass substrate. S1, S2 represent the electronic transitions for the semiconducting SWCNTs in the films, and M1 represents that of the metallic nanotubes. **g** Sheet resistance versus thickness of SWCNT films. The solid line is the best fit curve according to the definition of electrical conductivity [22]. Reprinted with permission from [22]. Copyright 2007 American Chemical Society

addition, the conductivity anisotropy could be regulated from 1 to 8 by increasing the film collection speed, resulting in more aligned bundles in the film.

5 Patterned Film Fabrication

Other than usual film manufacture, deposition of patterned films is another critical step for relevant final products such as touch panels and displays. Such patterning of CNT films can also overcome the tradeoff between transmittance and conductivity in TCFs. Patterned films are not uniformly transparent but may still meet many of the application requirements, as long as the features of the pattern are thin enough to not be recognized by the naked eye.

In the case of rectangular patterns, to a first-order approximation, the transmittance roughly equals the CNT coverage, while the conductance is proportional to the grid thickness:

$$R = \frac{\rho}{tf},$$

$$T = (1 - f) + f\mathrm{e}^{-\alpha t},$$

where R is the sheet resistance, T is the film transmittance, ρ is the resistivity of the CNT grid, t is the grid thickness, α is the absorption coefficient of the CNT grid, and f is the duty cycle of the grid pattern, viz. $f = \frac{W}{A}$, where W is the CNT grid width and A is the grid pitch (Fig. 6d). Instead of vanishing, the transmittance approaches $1 - f$ as the pattern becomes thicker. Therefore, conductance and transmittance are

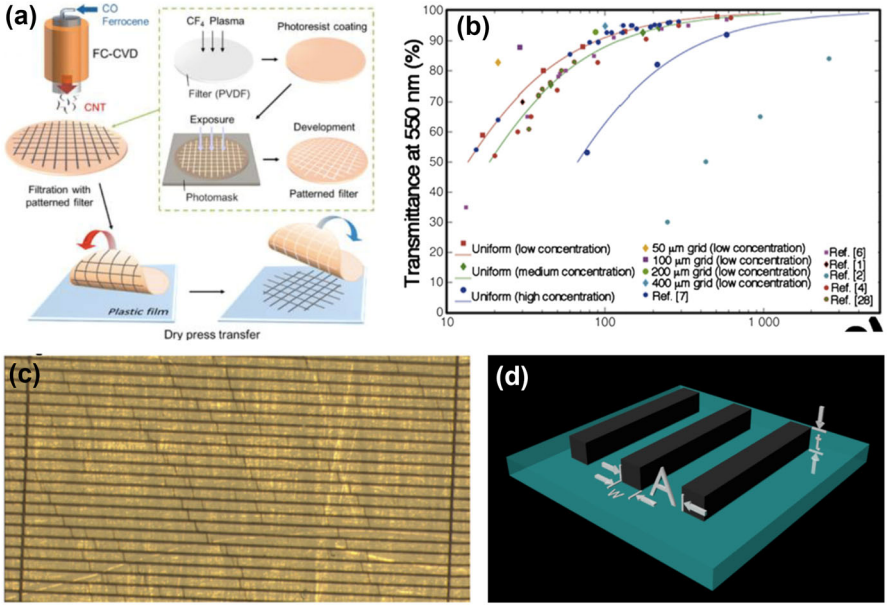

Fig. 6 Patterned carbon nanotube films: **a** Fabrication steps for patterned carbon nanotube film utilizing patterned filters [73]. Copyright 2014 American Chemical Society. **b** Comparison of sheet resistance between patterned and uniform carbon nanotube films and **c** optical image of patterned carbon nanotube films with rectangular geometry [33]. Copyright 2016 Elsevier. **d** Structural parameters of the rectangular pattern geometry

no longer strongly coupled. The factors limiting the conductivity are the quality of the CNTs and how thick the grid can be.

A few pioneering studies have been carried out on how to pattern carbon nanotube films. Inkjet printing is a facile method to make arbitrary patterns with linewidth above 50 microns [70]. On smaller scales, some specific patterns can be formed with the aid of polymer [71] or laser methods [72].

Among these methods, one approach is particularly well suited to the FCCVD method. This method utilizes dry transfer and photolithographically patterned filter membranes to achieve resolution down to microns, overcoming the tradeoff mentioned above. Fukaya et al. reported a 46% increase in conductivity for patterned compared with uniform film [73]. In a follow-up study, Kaskela et al. reported record-breaking performance of 69 Ω/sq at 97% transmittance [33].

Improving the uniform film quality still matters in the patterned case, since it provides better base material, achieving the target conductance with lower thickness and material consumption. The conductivity versus transmittance characteristic can be further improved if the pattern can be made thicker; For example, a 40-nm-thick film can transmit 75% of light at 550 nm [30], corresponding to an absorption coefficient of $\alpha = 72{,}000/\text{cm}$. Improvement in the carbon nanotube quality results in little change in film density, so the absorption coefficient remains roughly unaltered. However, improvement in tube–tube contact and length will reduce the film resistivity, as shown in a recent report in which films of individual carbon nanotubes reached 89 Ω/sq at 90% transmittance [33] with figure of merit of $\alpha\rho = 9.38$ and thus $\rho = 1.3 \times 10^{-6}\Omega \cdot m\,(or\,7700\,S \cdot cm)$. To achieve 10 Ω/sq at 90% transmittance, the grid thickness required is 1.3 microns. This thickness could be reduced further by applying better CNTs or through use of doping techniques, which will have lower $\alpha\rho$.

The value of 1.3 microns is not very thick for TCFs. However, few attempts have been made to form patterned random carbon nanotube films of such thickness. In previous attempts, the thickness of the densified film was around 0.15 microns, being limited by the thickness of the photoresist [73]. It is reasonable to expect that increasing the thickness of the photoresist, or development of new patterning techniques for thicker CNT films, will help CNT TCFs to reach better performance and wider application scenarios.

6 Characterization, requirements, and performance of CNT films fabricated by FCCVD for use as TCFs

Low sheet resistance and high light transmission across the UV−Vis–NIR spectrum are pursued for ideal transparent conducting films. Practically, sheet resistance can be measured directly using the four-point probe, two-point conductivity probe, or two-line method, while transmission can be obtained by measuring the UV−Vis absorbance of the TCF. Because the transmittance of a film decreases through absorption as its thickness is increased, there is a tradeoff between these two parameters [74]. Therefore, a figure of merit (FOM) should be defined to compare

various TCFs, combining transmission and sheet resistance and being independent of thickness.

According to existing literature, two main FOMs are used for comparison of TCFs [75], i.e., $\alpha\rho$ and σ_{dc}/σ_{OP}, where α, ρ, σ_{dc}, and σ_{OP} are the absorption coefficient, resistivity, direct-current (dc) electrical conductivity, and optical conductivity of a uniform TCF, respectively. The sheet resistance of a uniform film is defined as $R_s = \rho/t$, where t is the film thickness. According to the Beer–Lambert law, the transmission of light (T) through a film of homogeneous material can be modeled as $T = \exp(-\alpha t)$. Combining these two equations yields

$$T = \exp\left(-\frac{\alpha\rho}{R_s}\right). \tag{1}$$

$\alpha\rho$ is a constant parameter for a uniform and homogeneous material. In addition to Eq. (1), the following is another formula commonly used to describe the relationship between R_s and T for TCFs [76]:

$$T = \left(1 + \frac{Z_0}{2R_s}\frac{\sigma_{OP}}{\sigma_{dc}}\right)^{-2}, \tag{2}$$

where Z_0 is the characteristic impedance of vacuum ($\sim$376.73 Ω). Both σ_{dc} and σ_{OP} are fundamental properties of the material, therefore σ_{dc}/σ_{OP} is also a useful FOM for TCF evaluation. It is worth noting that Eq. (2) is based on the assumption that the film thickness is much less than the wavelength of interest. In the case of CNT films as TCFs, their thickness is generally <50 nm. Therefore, σ_{dc}/σ_{OP} is valid as a FOM to evaluate their performance of CNT films as TCFs. Degiorgi et al. measured a σ_{OP} value of 200 S/cm at 550 nm for buckypaper composed of SWNTs [77]. This value applies for SWNT films obtained by FCCVD, because σ_{OP} is independent of doping level but varies with the number of walls in the CNTs.

Good candidates for use in TCFs will have higher FOM, $\alpha\rho$ and σ_{dc}/σ_{OP}, meaning a material with high conductivity and low optical absorption [78]. Based on Eqs. (1) and (2), $\alpha\rho = \frac{Z_0}{2}\frac{\sigma_{OP}}{\sigma_{dc}}$ can be obtained by performing a Taylor expansion in T/R_s to first order. Hence, $\alpha\rho$ and σ_{dc}/σ_{OP} are phenomenologically equivalent. Because σ_{dc}/σ_{OP} is dimensionless and simple, we use it to compare the properties required for practical applications of CNT TCFs in Table 1.

The requirements on the optoelectronic properties of TCFs vary depending on the application [19]. The minimal requirements for practical application of TCFs are presented in Table 1. CNT films offer various advantages in terms of physical flexibility, excellent optical properties, and chemical stability, compared with ITO or other candidate TCFs. However, the conductivity of even state-of-the-art SWNT films must still be improved to meet industrial requirements for certain applications in order to replace ITO (Table 1); For example, transparent electrodes for photovoltaic devices require high transmittance above 90% and conductivity of R_s below 10 Ω/sq for efficient energy harvesting, which means $\frac{\sigma_{OP}}{\sigma_{dc}} > 348.5$. Based on theoretical and experimental results, the optoelectronic properties of SWNT films depend on many parameters, including the morphology (length, diameter, and

Table 1 Minimal requirements for practical applications of TCFs and performance of SWNT films as TCFs

TCF or application	T (%)	R_s (Ω/sq)	σ_{dc}/σ_{OP}	Comment	Refs.
Photovoltaic electrode	**90**	**10**	**348.5**		[19, 59]
ITO	90	10−100	348.5−34.8	Mature, low sheet resistance, high transparency; costly, brittle, high reflection	[19, 57]
Patterned SWNT film produced by FCCVD	97	69	178	Overcomes the tradeoff between T and R_s; costly, time-consuming	[33, 66]
	87	29	90		
MWNT film from CNT forest	83	24	80.4	Efficient process, less impurities, anisotropic conductivity; aligned CNT forest required, laser ablation and metal deposition	[29]
	90	208	16.8		
CNB film obtained by FCCVD	95	100	72.6	Mature, efficient process, good control over thickness; residual catalyst, chemical doping	[62]
OLED display electrode	**90**	**50**	**69.7**		[19, 59]
SWNT film obtained by liquid-phase processing	78−90	30−300	65-5	Fast and simple process, uniform films; chemical doping, high pollution	[19, 59, 106]
SWNT film deposited on filter by FCCVD	90	80−100	43.6−34.8	Mature, efficient process, laser ablation and metal deposition; residual catalyst, chemical doping	[31, 92, 126]
Individual SWNT film obtained by FCCVD	90	89	39.2	Better performance for thin-film transistors; low yield, time-consuming, short CNTs	[33, 98]
LCD screen electrode	**85**	**100**	**22.3**		[19, 59]
Enriched metallic SWCNT film obtained by FCCVD	90	160	21.8	88% M-SWNT, simple process; chemical doping, unclear mechanism	[49]
SWNT film deposited on reactor wall by FCCVD	70	50	19.3	Without further chemical doping, without hydrogen; poor uniformity, large-scale production limited, little control over thickness,	[22]
Continuous tubular SWNT film obtained by FCCVD	90	200	17.4	High yield, without hydrogen, without further chemical doping; high synthesis temperature, poor uniformity	[68]
Touch panel electrode	**85**	**500**	**4.5**		[19, 62]

The requirements of various applications for TCFs are in bold

orientation) of the SWNTs and bundles, the quality, purity, and chirality of the SWNTs, doping, etc. [79–82].

Since the contact resistance between individual SWNTs or bundles is orders of magnitude higher than the resistance along a tube [31, 81, 83, 84], highly resistive junctions limit the electrical conductivity of SWNT films obtained from FCCVD as well as other methods. Recently, Znidarsic et al. [85] used conductive atomic force microscopy to analyze the contact resistance between tubes at isolated junctions of

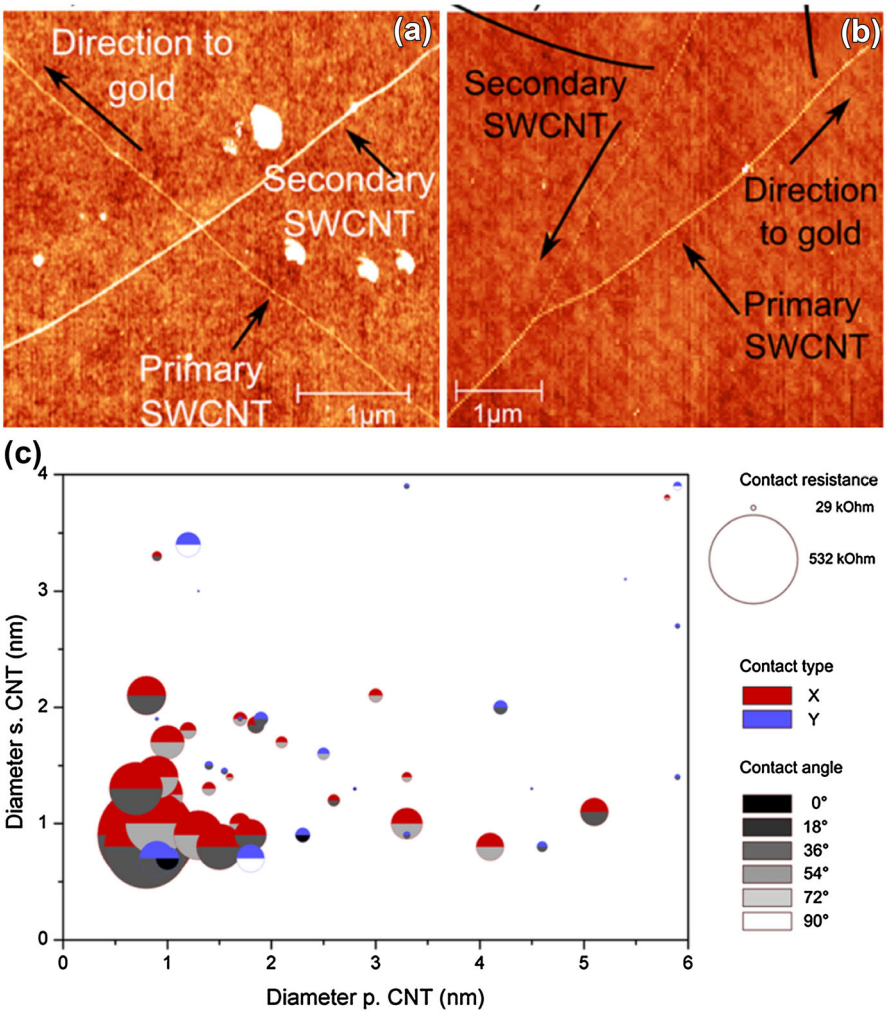

Fig. 7 Morphologies and contact resistances of SWCNT intermolecular junctions [85]. **a**, **b** AFM images of X and Y junctions, two main SWNT intermolecular junctions. **c** Contact resistance of X and Y junctions versus diameters of primary and secondary CNTs and their intersection angles. Y junctions have lower resistance than X junctions for given structural parameters, with minimum value of 29 kΩ. The contact resistance of both junctions is inversely proportional to the diameters of the CNT branches. Adapted with permission from [82]. Copyright 2014 American Chemical Society

pristine and nitric-acid-treated SWNT networks obtained by FCCVD, as shown in Fig. 7. At room temperature, the conductivity of a SWNT or bundle was found to be ohmic, with values close to 3–16 kΩ/μm. The resistance of their junctions was much higher, ranging from 29 to 532 kΩ and decreasing with increasing SWCNT or bundle diameter. The contact resistance also depended on the contact morphology [86]. Compared with X junctions, the contact resistance of Y junctions is orders of magnitude lower [15], because they benefit from carrier transport via longer interbundle connections. The contact resistance of both types of junction is inversely proportional to the diameters of CNT branches. They also found that moderate nitric acid treatment reduced the sheet resistance by a factor of 4 by reducing the average junction resistance by a factor of 3, while the resistance of the nanotubes remained largely unaltered. These results suggest that the mechanism for resistance reduction on doping is related to contact modulation with no major impact on the conductance of the SWNTs themselves [87]. However, in the case of defective or substitutionally doped SWNTs, the resistance of the SWNTs or their bundles may be much larger due to scattering on lattice defects, dominating the total resistance of the thin film [88, 89].

As mentioned above, interbundle and intertube contacts dominate the overall resistance of typical SWNT networks. Therefore, increasing bundle length correlates with decreasing sheet resistance at constant optical transparency, as longer bundles reduce the amount of high-resistance interbundle contacts in the network [90]. An exponential relationship between conductance and average CNT bundle length has been found experimentally [91]. Although longer CNTs do benefit fabrication of more conducting films, they are more difficult to disperse, particularly at high concentration. This intrinsic contradiction complicates and compromises many liquid-phase methods for CNT film fabrication. For the dry FCCVD method, however, no such problem exists. The length of the SWNTs produced depends on the residence time and growth rate, since SWNT growth occurs in a certain region (growth zone) in the FCCVD method. Kaskela et al. [31] deposited TCFs containing SWNT bundles of various lengths, synthesized in different reactors of various sizes based on the FCCVD method. With bundle length improvement from 1.3 μm to

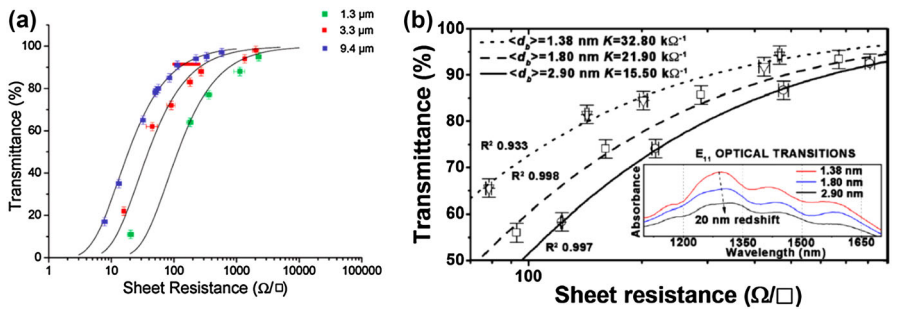

Fig. 8 Effect of bundle length and diameter on optoelectronic performance of SWNT films. With **a** increasing bundle length [31] or **b** decreasing bundle diameter [98], the performance of the SWNT films as TCFs was improved. Copyright 2010 American Chemical Society and Copyright 2009 AIP Publishing LLC

9.4 μm, the optoelectronic performance of the SWNT films was greatly improved, as shown in Fig. 8a. Moreover, a hybrid carbon source was applied to tune the bundle length based on different decomposition temperatures. Anoshkin et al. [92] fabricated SWNT films using a hybrid carbon source of CO and ethylene. SWNT film doped with gold chloride ($AuCl_3$) exhibited sheet resistance as low as 73 Ω/sq at transmittance of 90%. In addition, Reynaud et al. [93] obtained similar results when using toluene and ethylene as carbon sources. In general, use of a hydrocarbon carbon source leads to higher growth rate of CNTs compared with CO. For certain catalyst–carbon systems, use of appropriate additives including water, CO_2, sulfur, etc. can improve the CNT growth rate [37, 53, 94].

In addition to the nanotube or bundle length, the mean bundle size is expected to have a large, but relatively little understood effect on the performance of the resulting thin film. Due to van der Waals interactions between them, SWNTs have a strong tendency to aggregate into bundles during synthesis and processing. At the individual SWNT level, dielectric screening caused by adjacent SWNTs modulates the electronic properties of an SWNT. Optically, this can be observed as a redshift caused by decreased exciton lifetime.

Some work has been carried out on the dependence of the performance of thin films based on liquid processing on the bundle diameter. However, the conclusions are inconsistent, owing to the complex processes and numerous influencing factors. Hecht et al. [91] and Shin et al. [95]. studied the performance of films fabricated using vacuum filtration of SWNT dispersions, where the bundle length and diameter were controlled by using different sonication times. Hecht et al. could not reach reliable conclusions regarding the relation between bundle size and thin-film performance, because decreasing the bundle size also decreased the bundle length in their experimental procedure. However, Shin et al. claimed to be able to keep the bundle size and length more independent of each other, and concluded that the thin-film performance improved as the bundle size was decreased, for bundles of similar length. Lyons et al. [90] and Mustonen et al. [33] also considered the effect of bundling from a geometric viewpoint, using different commercially available SWNT dispersions and SWNTs synthesized using different floating catalyst CVD processes, respectively. They argued independently that decreasing the bundle diameter while keeping the optical density constant will increase the number of conductive pathways in the network and thereby the bulk electrical conductivity. However, this could be counteracted if the conductivity of bundles and especially the conductivity of junctions between them increases in proportion to the bundle size. Han et al. reported that conduction in large bundles can be constrained to the surface layer [96], meaning that the rest of the bundle contributes to optical absorption but not electrical conductivity. Likewise, contact resistances between bundles can be expected to be smaller than contact resistances between individual SWNTs due to their larger contact areas; this has been confirmed experimentally for nondoped tubes using conductive atomic force microscopy by Znidarsic et al. [85], although earlier study by Nirmalraj et al. [97] reached the opposite conclusion, possibly because their work used SWNTs deposited from a liquid dispersion and larger bundles could contain more contaminants. In the case of long rope-like structures, the intertube resistance inside the bundles themselves will also limit the

conductivity, although the contacts between them can be expected to be quite conductive due to the large contact areas between SWNTs arranged in this manner.

In contrast to liquid-phase processing, the bundle diameter can be controlled by regulating the catalyst and CNT concentration without affecting the length or chirality distribution when using FCCVD. Based on this fact, the aerosol CVD system can be used to reveal the essential relationship between film performance and bundle diameter. Mustonen et al. [98] studied the effect of bundle diameter (1.38, 1.80, and 2.90 nm) on TCE performance by deliberately aggregating aerosol-synthesized SWNTs in gas phase after synthesis [98], as shown in Fig. 8b. They concluded that films collected from a more bundled population of the same SWNTs performed worse and that the performance decrease could be described using a semiempirical model, assuming that the conductivity within the bundles is not higher compared with that in individual SWNTs, in accordance with Han et al. [96], and that the contact resistances between bundles are lower compared with those between individual SWNTs, in accordance with Znidarsic et al. [85]. Compared with earlier studies carried out using liquid dispersions, these experiments had the advantage that the properties of the individual SWNTs remained unchanged and the only variable was the amount of bundling. The conclusion that less bundled SWNTs are beneficial to improve the thin film conductivity is further supported by the studies of Mustonen et al. [42] and Kaskela et al. [33]. In these studies, the films fabricated from shorter (mean SWNT length 4 μm), nearly nonbundled SWNTs, displayed similar performance to earlier published films [31] consisting of longer SWNT bundles (mean bundle length 8–10 μm). The short SWNTs were synthesized at low concentration and thus undergoing almost no bundling during synthesis.

The ratio of metallic to semiconducting SWNTs in the network is also crucial to the film conductivity, based on two facts [99, 100]. Firstly, at room temperature, the resistance of an individual m-SWNT (10^{-4}–10^{-3} Ω cm) is much lower than that of its semiconducting counterpart (10 Ω cm) [101, 102]. In addition, the contact resistance of metal–semiconducting (M–S) heterojunctions is ∼1 MΩ at ambient temperature, one order of magnitude higher than for metal–metal (M–M) or semiconducting–semiconducting (S–S) junctions (∼20 kΩ) [86, 103], although doping is likely to reduce this difference [85]. Because of the nature of CNT networks as a mixture of semiconducting and metallic objects, almost all of the junctions are heterojunctions. Simulation results for the conductance versus proportion of semiconducting tubes of a SWNT thin film are shown in Fig. 9 [4]. Because of the low resistance of M−M and S−S contacts, the conductance of films composed of pure metallic or semiconducting tubes is quite high (point A and E). With increasing proportion of semiconducting SWNTs (from point A to point B), the conductance becomes dominated by Schottky barriers (M−S junctions) rather than metallic tubes. When the proportion of semiconducting tubes approaches 80% (point B to D), the conductance is blocked. For small amounts of metallic tubes in the network (from point D to E), the film conductivity increases as charges pass along paths formed by semiconducting SWNTs, bypassing the Schottky barriers. In 2014, Hou et al. [49] used the FCCVD method to prepare enriched m-SWNT films by introducing hydrogen as etchant gas. With increasing m-SWNT content, the

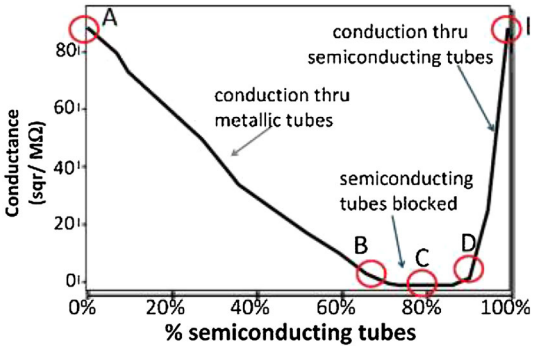

Fig. 9 Expected conductance as function of proportion of semiconducting tubes (assuming for simplicity that an unblocked semiconducting tube conducts as well as a metallic tube) [104]. Reprinted with permission from [101]. Copyright 2009 American Chemical Society. Conductance versus percentage of semiconducting CNTs in network, simulated for density three times the percolation threshold; CNT length, positions, and orientations are the same for different M/S ratios

sheet resistance at transmittance of 90% decreased from 500 Ω/sq to 160 Ω/sq, as shown in Fig. 9b.

7 Applications of SWNT Films in Touch Sensors and Display Electrodes

Transparent conducting films based on SWNTs are vital components in a range of electronic devices, such as touch screens [61, 62], LCDs [105, 106], OLEDs [107, 108], and solar cells [109, 110]. Currently, touch displays are the most mature application of SWNT TCFs [62], whereas most other applications of CNTs remain at laboratory stage. Resistive and capacitive touch panels can already be manufactured in factories and purchased on the market, indicating that practical applications of SWNT films have already started.

In 2013, Anisimov et al. [62] discussed recent progress in achieving characteristics and applications of TCFs based on Canatu's CNB technology. The combination of aerosol synthesis and direct dry printing allows homogeneous or patterned deposition on any substrate at room temperature and pressure, resulting in a simple, scalable, one-step, low-cost, and environmentally friendly thin-film manufacturing process that improves the quality and performance of final products. Direct dry printing is applicable to both sheet and roll-to-roll implementations and can be combined with conventional screen, gravure, and flexo printing to enable production of continuous rolls of complex, multilayered components. These advances are significant because they will enable flexible and even three-dimensional (3D)-shaped touch sensors, high-optical-quality touch displays with almost no reflection and high outdoors contrast, and cost-effective manufacturing through dry roll-to-roll processing.

Deposition of homogeneous and patterned CNB films can be achieved by combining the aerosol synthesis method with room-temperature deposition based on a modification of the aforementioned filter transfer technique. The conductivity of

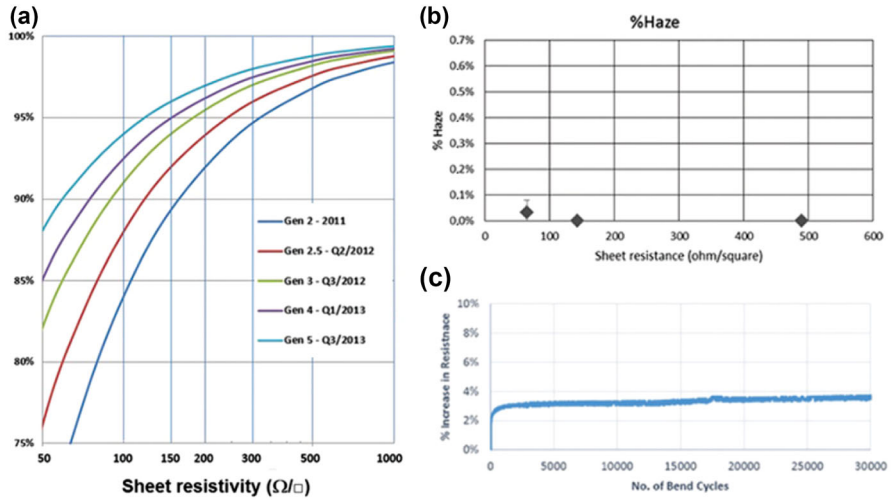

Fig. 10 **a** CNB film transmission versus sheet resistivity, comparing current Gen 5 with previous results from 2011 to 2013. Transmission is substrate-normalized. **b** Haze of substrate-normalized CNB films as function of sheet resistivity. Haze does not increase at low sheet resistivity as it does with AgNW and metal meshes. **c** Change in resistivity of CNB film on 130-μm PET substrate after repeated bends to radius of 2 mm [62]. Copyright 2014 Society for Information Display

CNB films of given transparency has doubled approximately every 12 months since 2007. Figure 10a shows CNB film releases since 2011. High transparency is needed to enable bright display images and pattern invisibility. In 2013, Gen 5 films with the following properties without substrate were reported: 100 Ω/sq at 94%, 150 Ω/sq at 96%, and 270 Ω/sq at 98%. In addition, film performance has reached up to 100 Ω/sq at $> 95\%$ in the laboratory [62].

CNT films have therefore been found to be low haze, neutrally colored, uniform, and both environmentally and mechanically stable.

Figure 10b shows the haze of substrate-normalized CNB films as a function of sheet resistivity. The haze of CNB film is negligible ($< 0.1\%$) and does not increase at low sheet resistivity as it does with AgNW and metal meshes. The optical absorption of CNB film is uniform over the entire visible spectrum. The Commission Internationale de l'Éclairage (CIE) *Lab* color coordinates after normalization were measured as $L^* = 97.9 \pm 0.1$, $a^* = 0.0 \pm 0.1$, and $b^* = 0.6 \pm 0.1$, demonstrating that CNB films and sensors have very little color distortion. TCF stability is also critical in practical applications, because fabrication and operation of actual devices may involve various levels of temperature and humidity. CNB films have been evaluated using all typical consumer electronics environmental tests. As shown by the results in Table 2, they passed these standard tests when using both environmental and accelerated aging. Experiments on mechanical stability have also been carried out to evaluate the applicability of CNBs for flexible and foldable electronics. The results for CNB film on 130-μm-thick PET substrate exposed to severe (180°) bending to radius of 2 mm are shown in Fig. 10c. The sheet resistance remained nearly constant over 30,000 bending cycles, after an

Table 2 Test results on CNB films including both environmental and accelerated aging [62]. Copyright 2014 Society for Information Display

		Specification				
Test	Standard	ΔR_s (sheet resistivity change)	$\Delta\%T$ (transmission change)	ΔHaze	ΔE (color change)	Adhesion (cross-cut and tape peel-off, JIS K5600)
Room-temperature storage	25 °C/60% RH	Passed	Passed	Passed	Passed	Passed
Constant-temperature/humidity storage	IEC 68-2-78 (IEC 68-2-3) 60 °C/90% RH	Passed	Passed	Passed	Passed	Passed
Thermal cycle storage	IEC 68-2-2, IEC 60068-2-14 Test N, IEC 60068-2-2 Na, 40 °C	Passed	Passed	Passed	Passed	Passed
High-temperature storage	IEC 68-2-2, IEC 60068-2-2 dry heat tests, 85 °C	Passed	Passed	Passed	Passed	Passed
Low-temperature storage	IEC 68-2-1–40 °C	Passed	Passed	Passed	Passed	Passed

initial change of a few percent. In another similar test with 140,000 bending cycles, the change in resistivity was less than 7%. The Canatu facility allows capacity of up to 500,000 m^2/month. Together, these results indicate that CNB films can indeed be used as a substitute for ITO electrodes in consumer electronics.

Most touch sensors and displays require fine patterning with minimum feature sizes of 25–50 μm. For ITO, photolithography with eight steps is commonly used for such fine patterning. However, fine patterning of CNB films is achieved via laser ablation, which maintains the dry manufacturing process with no liquid handling and hence a lower environmental footprint. Because no masks and only one process step are required in laser ablation, the time and cost are competitive. In addition, the low incremental capital expenditure for laser equipment as opposed to a photolithography line makes it more flexible in the face of demand fluctuations and enables better line utilization. Ag traces are also fine-patterned to 30 μm/30 μm lines and gaps, either by laser ablation in the same process step as the CNB patterning or, for even better production efficiency, by direct screen printing. It is important to note that metal-mesh-based touch sensors require very high tolerance

and early design knowhow of display pixel geometry to reduce the moiré effect between the display and sensor. Metal mesh manufacture is also demanding, as the bonding equipment needs to be tightly controlled. CNB sensors are display design agnostic due to the pattern invisibility and random orientation of CNB deposition.

Based on the availability of flexible and cost-effective CNB films with excellent and stable performance, touch sensors (Fig. 11) and high-optical-quality touch displays (Fig. 12) have been manufactured. Specifically, a CNB-based two-layer glass–film–film (GFF) structure demonstrator was created, showing only 2.2% reflection and 40% better contrast in bright ambient light compared with a comparable structure using ITO. For 3D-shaped rigid touch sensing, formability with 1 mm radius edges and 120% stretching was achieved.

The 13.3-inch-diagonal CNB projected-capacitive touch sensors were manufactured (Fig. 12b) based on the process shown in Fig. 12a. The touch stack was of glass–film–film (GFF) type with sense and drive electrodes on separate PET sheets, laminated together and to the front glass using optically clear adhesive. The CNB film sheet resistivity was 220 Ω/sq. The sensors were bonded with a flexible circuit board to the driving electronics, and the touch module assembly was "plug and play" retrofitted to an existing Intel Ultrabook reference design for comparison with the existing standard commercial ITO One Glass Sensor (OGS). An Atmel mXT224 chip was used as touch controller. The CNB touch sensor passed Windows Hardware Certification Kit (WHCK) tests and is therefore fully certified for Windows 8. As characterized by Atmel, the touch performance was found to be equivalent to commercial ITO sensors. The reflectivity from the CNB GFF touch display was significantly lower than that from the comparison ITO OGS touch display. The optical characterization of various touch modules is presented in

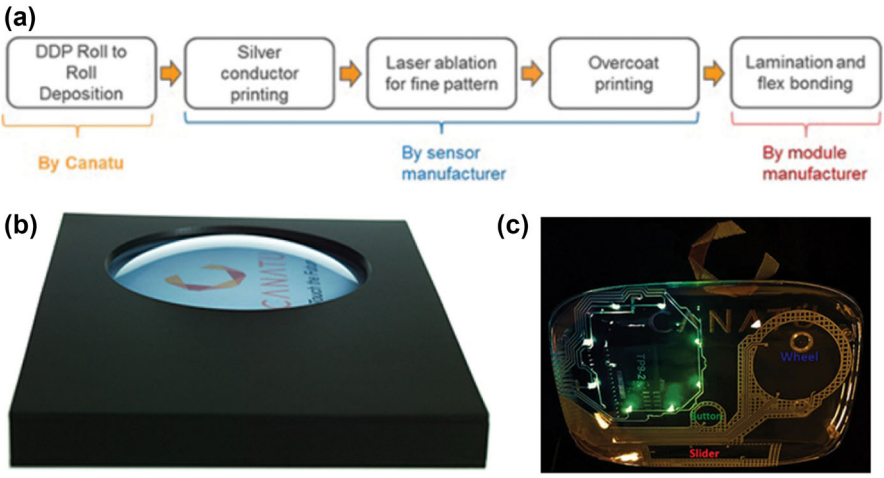

Fig. 11 Touch sensor based on CNB film [62]. Copyright 2014 Society for Information Display. **a** CNB touch sensor manufacturing process and business model for high-volume touch sensor sales. **b** Dome-shaped CNB projected-capacitive multitouch sensor. **c** 3D-shaped CNB FIM demonstrator with touch

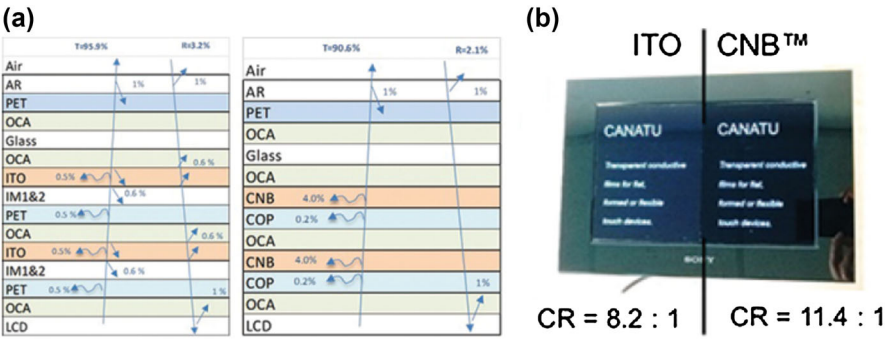

Fig. 12 **a** Stack diagram of touch display direct-bonded 150 Ω/sq ITO GFF (left) compared with CNB GFF (right). **b** ITO and CNB touch display [62]. The demonstrator is shown on the far right. Copyright 2014 Society for Information Display

Table 3 Optical characterization in terms of haze for touch modules with a variety of transparent conductors [62]. Copyright 2014 Society for Information Display

Touch module	Type	Sensor	Haze (%)
Carbon NanoBud	CNB	GFF	0.6
ITO OGS (no index matching)	ITO	OGS	3.3
Silver nanowire metal mesh	Mesh	GFF	1.4
Silver metal mesh #1	Mesh	GFF	2.0
Copper metal mesh #1	Mesh	GF2	1.6
Copper metal mesh #2	Mesh	GF2	2.0
Silver metal mesh #2	Mesh	GF2	1.3
iPAD 4 (air)	ITO	GF2	1.0

Table 3. Compared with ITO and metal mesh touch modules, CNB touch modules have the lowest haze.

A highly transparent 3D-shaped demonstrator with slider, wheel, and button touch was also created (Fig. 12c), based on the FIM process with CNB on thin polycarbonate substrate and clear poly(methyl methacrylate) overmold. The radius of curvature was 130 mm. For rigid 3D-shaped touch devices, film insert molding (FIM) as a standard industrial process was applied. The 120% stretching and 87° bending at 1 mm radius of the FIM device demonstrate the high stretchability of CNB films. Both one- and two-CNB-layer test devices for plastic–film (PF1)- and plastic–film–film (PFF)-type touch stack constructions were made. CNB layers, applied on polycarbonate Makrofol DE film, were 3D-shaped using a high-pressure forming process. The resulting inserts were injection back-molded with clear Makrolon polycarbonate resin. In all test devices, the CNB layers maintained their conductivity with linear response to stretching.

To demonstrate touch display contrast in a direct-bonded construction, 10-inch optical demonstrators of TFT LCD touch panels were also made (Fig. 12) with two types: an ITO-based 150 Ω/sq GFF stack and a 150 Ω/sq CNB GFF stack. As presented in Table 4, the CNB GFF device exhibited 2.2% total reflectance, whereas the total reflectance from the ITO GFF device was 3.4%. Table 4 presents a

Table 4 Specular and diffuse reflection results for CNB and ITO GFF optical demonstrators with AR coating [62]. Copyright 2014 Society for Information Display

Direct-bonded touch module	Specular reflection (%)	Diffuse reflection (%)	Total reflection (%)
CNB AR/GFF	1.85	0.36	2.21
ITO AR/GFF	2.91	0.47	3.38

breakdown of the reflection values in the touch display structure. The CNB sensor stack showed no inherent reflections, hence the 1.8% specular reflection for the GFF stack originated from the glass–antireflection (AR) coating–air interface and from the display (Fig. 8). For the ITO sensor stack, despite complex index-matching layers, 1% specular reflection from the ITO layers was still observed. By better optimizing the AR coating, using a less reflective display, and optimizing the direct bonding materials, $< 1\%$ specular reflection is feasible with CNB GFF sensors.

Demonstrators of touch and display devices have therefore been successfully produced, indicating that CNB films are now a commercially viable option for high-volume applications and for high-quality flat, flexible, and 3D-formed touch sensors for use in mobile phones, tablets, phablets, laptops, smart watches, digital cameras, automotive consoles, and white goods.

8 Summary and Outlook

This review has described recent developments in SWNT thin films fabricated by dry methods based on FCCVD, including SWNT synthesis and film fabrication, properties, and applications as TCFs. As an emerging class of materials, SWNT thin films possess unique optical transparency and superior electric properties and mechanical flexibility, resulting from not only the incorporation of individual SWNTs but also their collective behavior, with additional properties arising from tube–tube interactions. Among these promising candidate materials, CNT TCFs exhibit great potential because of their chemical stability, high stretchability, color neutrality and less haze, wider spectral range, etc. [56, 59, 67]. Compared with liquid-phase processing, which involves various time- and resource-consuming steps, dry FCCVD methods without dispersion in solution are more direct and simpler. By avoiding the tradeoff between CNT length and solubility during film fabrication, the dry FCCVD method enables production of films that contain longer CNTs and exhibit excellent optoelectronic properties. Films based on SWNTs produced by the dry FCCVD method are already commercially available for application in touch and display devices. However, the transparent and conductive properties of these CNT films must be further improved to expand their application scope, e.g., to include solar cells.

In the dry FCCVD method, control of the CNT morphology and chirality is critical to improve the film performance. Increasing the bundle length and reducing the diameter, down to individual tube level, can effectively improve the film conductivity. The length of the SWNTs or bundles depends on the growth time and

growth rate during the synthesis. Limiting the number concentration of CNTs in gas phase prevents nanotube collision and bundle formation. With increasing aspect ratio of CNTs and bundles, it becomes very important to maintain a stable laminar gas flow, to prevent formation of CNT and bundle loops, which would greatly reduce the effect of greater CNT length. Controlled synthesis of CNTs is still in the development stage, with further research efforts needed. Although there are some papers on direct or posttreatment methods to synthesize or separate pure metallic or semiconducting CNTs [31, 49, 52, 111, 112], scalable and reliable methods are still desired for further commercialization in CNT applications. Separation of tubes based on their electric conductivity would benefit applications in transparent conductors and thin-film transistors [113], another major application for CNT films. Considering the difficulty of obtaining high-purity semiconducting CNTs [112], CNT film transistor technology remains at an earlier stage compared with transparent conductors. In addition to the neat material, extensive investigations on numerous dopants for CNTs have been carried out. The effectiveness of doping for improving the conductance of CNT films has been demonstrated. However, stability issues and the effects of functional groups and residual dopant on device performance have been less well studied and evaluated [114, 115], being critical for actual device applications and commercial use.

Research on the dry FCCVD method for fabrication of SWNT films could advance the development of not only industrial applications but also the fundamental science of related nanostructured materials and nanodevices. Except for transparent electrodes and thin-film transistors, SWNT films produced by the dry FCCVD method also have great potential for use in several other high-impact applications, including sensors [116–118], ultrafast femtosecond lasers [30, 119–121], thermoacoustic loudspeakers [122], energy storage [123–125], etc. We believe that SWNT films produced by the dry FCCVD method will soon be an essential component in commercial device applications, because of not only their unique properties and low cost but also promising research results.

Acknowledgements We acknowledge financial support from the European Union Seventh Framework Programme (FP7/2007-2013) under Grant Agreement No. 604472 (IRENA project), the Aalto Energy Efficiency (AEF) Research Program through the MOPPI project, TEKES of Finland via CNT-PV project, and Academy of Finland via projects 286546 and 292600.

References

1. de Volder MFL, Tawfick SH, Baughman RH, Hart AJ (2013) Carbon nanotubes: present and future commercial applications. Science 339:535–539
2. Iijima S, Ichihashi T (1993) Single-shell carbon nanotubes of 1-nm diameter. Nature 363:603–605
3. Ijiima S (1991) Helical microtubules of graphitic carbon. Nature 354:56–58
4. Dresselhaus MS, Dresselhaus G, Saito R (1995) Physics of carbon nanotubes. Carbon N. Y. 33:883–891
5. Saito R et al (2001) Chirality-dependent G-band Raman intensity of carbon nanotubes. Phys Rev B 64:853121–853127
6. Cheng HM, Li F, Sun X, Brown SDM, Pimenta MA, Marucci A, Dresselhaus G, Dresselhaus MS (1998) Bulk morphology and diameter distribution of single-walled carbon nanotubes synthesized by catalytic decomposition of hydrocarbons. Chem Phys Lett 289:602–610

7. Saito R, Fujita M, Dresselhaus G, Dresselhaus MS (1992) Electronic structure of graphene tubules based on C60. Phys Rev B 46:1804–1811
8. Kane CL, Mele EJ (1997) Size, shape, and low energy electronic structure of carbon nanotubes. Phys Rev Lett 78:1932
9. Yao Z, Kane CL, Dekker C (2000) High-field electrical transport in single-wall carbon nanotubes. Phys Rev Lett 84:2941–2944
10. Zhou X, Park JJY, Huang S, Liu J, McEuen PPL (2005) Band structure, phonon scattering, and the performance limit of single-walled carbon nanotube transistors. Phys Rev Lett 95:146805
11. Pop E, Mann D, Wang Q, Goodson K, Dai HJ (2006) Thermal conductance of an individual single-wall carbon nanotube above room temperature. Nano Lett 6:96–100
12. Pan ZW et al (1999) Tensile tests of ropes of very long aligned multiwall carbon nanotubes. Appl Phys Lett 74:3152–3154
13. Yu M (2000) Strength and breaking mechanism of multiwalled carbon nanotubes under tensile load. Science 287:637–640
14. Hu L, Hecht DS, Gru G (2010) Carbon nanotube thin films: fabrication, properties, and applications. Chem Rev 499:5790–5844
15. Ma W et al (2009) Monitoring a micromechanical process in macroscale carbon nanotube films and fibers. Adv Mater 21:603–608
16. Brieland-Shoultz A et al (2014) Scaling the stiffness, strength, and toughness of ceramic-coated nanotube foams into the structural regime. Adv Funct Mater 24:5728–5735
17. Zhou W, Bai X, Wang E, Xie S (2009) Synthesis, structure, and properties of single-walled carbon nanotubes. Adv Mater 21:4565–4583
18. Zhang Q et al (2017) Performance improvement of continuous carbon nanotube fibers by acid treatment. Chin Phys B 26:28802
19. Yu L, Shearer C, Shapter J (2016) Recent development of carbon nanotube transparent conductive films. Chem Rev 116:13413–13453
20. Cao Q, Rogers JA (2009) Ultrathin films of single-walled carbon nanotubes for electronics and sensors: a review of fundamental and applied aspects. Adv Mater 21:29–53
21. Zhou W, Ma W, Niu Z, Song L, Xie S (2012) Freestanding single-walled carbon nanotube bundle networks: fabrication, properties and composites. Chin Sci Bull 57:205–224
22. Ma W et al (2007) Directly synthesized strong, highly conducting, transparent single-walled carbon nanotube films. Nano Lett 7:2307–2311
23. Wu Z et al (2004) Transparent, conductive carbon nanotube films. Science 305:1273–1276
24. Mirri F et al (2012) High-performance carbon nanotube transparent conductive films by scalable dip coating. ACS Nano 6:9737–9744
25. Cao Q et al (2006) Highly bendable, transparent thin-film transistors that use carbon-nanotube-based conductors and semiconductors with elastomeric dielectrics. Adv Mater 18:304–309
26. Liu B et al (2009) Metal-catalyst-free growth of single-walled carbon nanotubes. J Am Chem Soc 131:2082–2083
27. Zhang L et al (2017) Selective growth of metal-free metallic and semiconducting single-wall carbon nanotubes. Adv Mater. https://doi.org/10.1002/adma.201605719
28. Zhang M (2005) Strong, transparent, multifunctional, carbon nanotube sheets. Science 309:1215–1219
29. Feng C et al (2010) Flexible, stretchable, transparent conducting films made from superaligned carbon nanotubes. Adv Funct Mater 20:885–891
30. Nasibulin AG et al (2011) Multifunctional free-standing single-walled carbon nanotube films. ACS Nano 5:3214–3221
31. Kaskela A et al (2010) Aerosol-synthesized SWCNT networks with tunable conductivity and transparency by a dry transfer technique. Nano Lett 10:4349–4355
32. Nasibulin AG et al (2008) Integration of single-walled carbon nanotubes into polymer films by thermo-compression. Chem Eng J 136:409–413
33. Kaskela A et al (2016) Highly individual SWCNTs for high performance thin film electronics. Carbon N Y 103:228–234
34. Baughman RH (2002) Carbon nanotubes-the route toward applications. Science 297:787–792
35. Nasibulin AG, Moisala A, Brown DP, Jiang H, Kauppinen EI (2005) A novel aerosol method for single walled carbon nanotube synthesis. Chem Phys Lett 402:227–232

36. Bronikowski MJ, Willis PA, Colbert DT, Smith KA, Smalley RE (2001) Gas-phase production of carbon single-walled nanotubes from carbon monoxide via the HiPco process: a parametric study. J Vac Sci Technol 19:1800–1805
37. Li Y-L (2004) Direct spinning of carbon nanotube fibers from chemical vapor deposition synthesis. Science 304:276–278
38. Gui X et al (2010) Soft, highly conductive nanotube sponges and composites with controlled compressibility. ACS Nano 4:2320–2326
39. Lamouroux E, Serp P, Kalck P (2007) Catalytic routes towards single wall carbon nanotubes. Catal Rev 49:341–405
40. Barnard JS, Paukner C, Koziol KK (2016) The role of carbon precursor on carbon nanotube chirality in floating catalyst chemical vapour deposition. Nanoscale 8:17262–17270
41. Moisala A, Nasibulin AG, Kauppinen EI (2003) The role of metal nanoparticles in the catalytic production of single-walled carbon nanotubes. J Phys Condens Matter 15(42):3011
42. Mustonen K et al (2015) Gas phase synthesis of non-bundled, small diameter single-walled carbon nanotubes with near-armchair chiralities. Appl Phys Lett 107:013106
43. Cheng HM et al (1998) Large-scale and low-cost synthesis of single-walled carbon nanotubes by the catalytic pyrolysis of hydrocarbons. Appl Phys Lett 72:3282–3284
44. Li Y-L, Zhang L-H, Zhong X-H, Windle AH (2007) Synthesis of high purity single-walled carbon nanotubes from ethanol by catalytic gas flow CVD reactions. Nanotechnology 18:225604
45. Chen Z et al (2004) An enhanced CVD approach to extensive nanotube networks with directionality. Carbon N Y 12:275504
46. He M, Jiang H, Kauppinen EI, Lehtonen J (2012) Diameter and chiral angle distribution dependencies on the carbon precursors in surface-grown single-walled carbon nanotubes. Nanoscale 4:7394
47. Harutyunyan AR et al (2009) Preferential growth of single-walled carbon nanotubes with metallic conductivity. Science 326:116–120
48. Vilatela JJ, Windle AH (2010) Yarn-like carbon nanotube fibers. Adv Mater 22:4959–4963
49. Hou PX et al (2014) Preparation of metallic single-wall carbon nanotubes by selective etching. ACS Nano 8:7156–7162
50. Piao Y et al (2016) Intensity ratio of resonant Raman modes for (n, m) enriched semiconducting carbon nanotubes. ACS Nano 10:5252–5259
51. Jiang H, Nasibulin AG, Brown DP, Kauppinen EI (2007) Unambiguous atomic structural determination of single-walled carbon nanotubes by electron diffraction. Carbon N Y 45:662–667
52. He M et al (2013) Chiral-selective growth of single-walled carbon nanotubes on lattice-mismatched epitaxial cobalt nanoparticles. Sci Rep 3:1460
53. Nasibulin AG et al (2006) An essential role of CO_2 and H_2O during single-walled CNT synthesis from carbon monoxide. Chem Phys Lett 417:179–184
54. Moisala A et al (2006) Single-walled carbon nanotube synthesis using ferrocene and iron pentacarbonyl in a laminar flow reactor. Chem Eng Sci 61:4393–4402
55. Nasibulin AG et al (2007) A novel hybrid carbon material. Nat Nanotechnol 2:156–161
56. Hecht DS, Hu L, Irvin G (2011) Emerging transparent electrodes based on thin films of carbon nanotubes, graphene, and metallic nanostructures. Adv Mater 23:1482–1513
57. Ellmer K (2012) Past achievements and future challenges in the development of optically transparent electrodes. Nat Photon 6:809–817
58. Chang DS, Lai ST (2015) Implementation of cross-generation automation transportation system in the TFT-LCD industry. Int J Adv Manuf Technol 78:753–763
59. Du J, Pei S, Ma L, Cheng HM (2014) 25th anniversary article: carbon nanotube- and graphene-based transparent conductive films for optoelectronic devices. Adv Mater 26:1958–1991
60. Feldman D et al. (2015) Shared solar: current landscape, market potential, and the impact of federal securities regulation (No. NREL/TP–6A20-63892). National Renewable Energy Lab.(NREL), Golden, CO (United States)
61. Hecht DS et al (2009) Carbon-nanotube film on plastic as transparent electrode for resistive touch screens. J Soc Inf Disp 17:941
62. Anisimov AS, Brown DP, Mikladal BF, Liam Ó (2014) Printed touch sensors using carbon NanoBud material. *Soc. Inf. Disp. Tech. Dig.* 1–8
63. Garnett EC et al (2012) Self-limited plasmonic welding of silver nanowire junctions. Nat Mater 11:241–249
64. Lee JY, Connor ST, Cui Y, Peumans P (2008) Solution-processed metal nanowire mesh transparent electrodes. Nano Lett 8:689–692

65. Li X et al (2009) Large-area synthesis of high quality and uniform graphene films on copper foils. Science 324:1312–1314
66. Fukaya N et al (2014) One-step sub-10 μm patterning of carbon-nanotube thin films for transparent conductor applications. ACS Nano 8:3285–3293
67. Sun D-M et al (2013) Mouldable all-carbon integrated circuits. Nat Commun 4:1–8
68. Zhou W, Zhang Q, Wang Y, Xie S (2014) Ultrathin carbon nanotube film and preparation method and device thereof. U.S. Patent Application No. 14/889,753
69. Gonzalez D et al (2005) A new thermophoretic precipitator for collection of nanometer-sized aerosol particles. Aerosol Sci Technol 39:1064–1071
70. Yu L, Shearer C, Shapter J (2016) Recent development of carbon nanotube transparent conductive films. Chem Rev. https://doi.org/10.1021/acs.chemrev.6b00179
71. Dionigi C et al (2007) Carbon nanotube networks patterned from aqueous solutions of latex bead carriers. J Mater Chem 17:3681
72. Castro MRS, Lasagni AF, Schmidt HK, Mücklich F (2008) Direct laser interference patterning of multi-walled carbon nanotube-based transparent conductive coatings. Appl Surf Sci 254:5874–5878
73. Fukaya N, Kim DY, Kishimoto S, Noda S, Ohno Y (2014) One-step sub-10 μm patterning of carbon-nanotube thin films for transparent conductor applications. ACS Nano 8:3285–3293
74. Zhou W et al (2004) Single wall carbon nanotube fibers extruded from super-acid suspensions: preferred orientation, electrical, and thermal transport. J Appl Phys 95:649–655
75. Dan B, Irvin GC, Pasquali M (2009) Continuous and scalable fabrication of transparent conducting carbon nanotube films. ACS Nano 3:835–843
76. Hu L, Hecht DS, Grüner G (2004) Percolation in transparent and conducting carbon nanotube networks. Nano Lett 4:2513–2517
77. Ruzicka B, Degiorgi L (2000) Optical and dc conductivity study of potassium-doped single-walled carbon nanotube films. Phys Rev B 61:R2468–R2471
78. Bergin SD et al (2008) Towards solutions of single-walled carbon nanotubes in common solvents. Adv Mater 20:1876–1881
79. Tian Y et al (2010) Analysis of the size distribution of single-walled carbon nanotubes using optical absorption spectroscopy. J Phys Chem Lett 1:1143–1148
80. King PJ, Higgins TM, De S, Nicoloso N, Coleman JN (2012) Percolation effects in supercapacitors with thin, transparent carbon nanotube electrodes. ACS Nano 6:1732–1741
81. De S, King PJ, Lyons PE, Khan U, Coleman JN (2010) Size effects and the problem with percolation in nanostructured transparent conductors. ACS Nano 4:7064–7072
82. De S, Coleman JN (2011) The effects of percolation in nanostructured transparent conductors. MRS Bull 36:774–781
83. Harris JM et al (2012) Electronic durability of flexible transparent films from type-specific single-wall carbon nanotubes. ACS Nano 6:881–887
84. Timmermans MY et al (2012) Effect of carbon nanotube network morphology on thin film transistor performance. Nano Res 5:307–319
85. Znidarsic A et al (2013) Spatially resolved transport properties of pristine and doped single-walled carbon nanotube networks. J Phys Chem C 117:13324–13330
86. Farajian AA, Esfarjani K, Kawazoe Y (1999) Nonlinear coherent transport through doped nanotube junctions. Phys Rev Lett 82:5084–5087
87. Shin D-W et al (2009) A role of HNO_3 on transparent conducting film with single-walled carbon nanotubes. Nanotechnology 20:475703
88. Susi T et al (2011) Nitrogen-doped single-walled carbon nanotube thin films exhibiting anomalous sheet resistances. Chem Mater 23:2201–2208
89. Geng H-Z et al (2007) Effect of acid treatment on carbon nanotube-based flexible transparent conducting films. J Am Chem Soc 129:7758–7759
90. Lyons PE et al (2008) The relationship between network morphology and conductivity in nanotube films. J Appl Phys 104:044302
91. Hecht D, Hu L, Grüner G (2006) Conductivity scaling with bundle length and diameter in single walled carbon nanotube networks. Appl Phys Lett 89:133112
92. Anoshkin IV et al (2014) Hybrid carbon source for single-walled carbon nanotube synthesis by aerosol CVD method. Carbon N Y 78:130–136
93. Reynaud O et al (2014) Aerosol feeding of catalyst precursor for CNT synthesis and highly conductive and transparent film fabrication. Chem Eng J 255:134–140

94. Hata K et al (2004) Water-assisted highly efficient synthesis of impurity-free single-walled carbon nanotubes. Science 306:1362–1364
95. Shin DH, Shim HC, Song JW, Kim S, Han CS (2009) Conductivity of films made from single-walled carbon nanotubes in terms of bundle diameter. Scr Mater 60:607–610
96. Han J-H, Strano MS (2014) Room temperature carrier transport through large diameter bundles of semiconducting single-walled carbon nanotube. Mater Res Bull 58:1–5
97. Nirmalraj PN, Lyons PE, De S, Coleman JN, Boland JJ (2009) Electrical connectivity in single-walled carbon nanotube networks. Nano Lett 9:3890–3895
98. Mustonen K et al (2015) Uncovering the ultimate performance of single-walled carbon nanotube films as transparent conductors. Appl Phys Lett 107:1–6
99. Blackburn JL et al (2008) Transparent conductive single-walled carbon nanotube networks with precisely tunable ratios of semiconducting and metallic nanotubes. ACS Nano 2:1266–1274
100. Rother M, Schießl SP, Zakharko Y, Gannott F, Zaumseil J (2016) Understanding charge transport in mixed networks of semiconducting carbon nanotubes. ACS Appl Mater Interfaces 8:5571–5579
101. Zhang WJ, Zhang QF, Chai Y, Shen X, Wu JL (2007) Carbon nanotube intramolecular junctions. Nanotechnology 18:395205
102. Ouyang M (2001) Atomically resolved single-walled carbon nanotube intramolecular junctions. Science 291:97–100
103. Stadermann M et al (2004) Nanoscale study of conduction through carbon nanotube networks. Phys Rev B 69:201402
104. Topinka MA, Rowell MW, Goldhaber-gordon D, Mcgehee MD, Gruner G (2009) Charge transport in interpenetrating networks of semiconducting and metallic carbon nanotubes. Nano Lett 9:2–4
105. Hayes RA, Feenstra BJ (2003) Video-speed electronic paper based on electrowetting. Nature 425:383–385
106. Park Y, Hu L, Gruner G, Irvin G, Drzaic P (2008) 37.4: late-news paper : integration of carbon nanotube transparent electrodes into display applications. Sid Dig. https://doi.org/10.1889/1.3069721
107. Zhang D et al (2006) Transparent, conductive, and flexible carbon nanotube films and their application in organic light-emitting diodes. Nano Lett 6:1880–1886
108. Li J et al (2006) Organic light-emitting diodes having carbon nanotube anodes. Nano Lett 6:2472–2477
109. Trancik JE, Barton SC, Hone J (2008) Transparent and catalytic carbon nanotube films. Nano Lett 8:982–987
110. Park J-U et al (2007) High-resolution electrohydrodynamic jet printing. Nat Mater 6:782–789
111. Yang F et al (2014) Chirality-specific growth of single-walled carbon nanotubes on solid alloy catalysts. Nature 510:522–524
112. Krupke R, Hennrich F, Löhneysen HV, Kappes MM (2003) Separation of metallic from semiconducting single-walled carbon nanotubes. Science 301:344–347
113. Park S, Vosguerichian M, Bao Z (2013) A review of fabrication and applications of carbon nanotube film-based flexible electronics. Nanoscale 5:1727
114. Jackson R, Domercq B, Jain R, Kippelen B, Graham S (2008) Stability of doped transparent carbon nanotube electrodes. Adv Funct Mater 18:2548–2554
115. Doherty EM et al (2009) The spatial uniformity and electromechanical stability of transparent, conductive films of single walled nanotubes. Carbon N Y 47:2466–2473
116. Lipomi DJ et al (2011) Skin-like pressure and strain sensors based on transparent elastic films of carbon nanotubes. Nat Nanotechnol 6:788–792
117. Cai L et al (2012) Highly transparent and conductive stretchable conductors based on hierarchical reticulate single-walled carbon nanotube architecture. Adv Funct Mater 22:5238–5244
118. Kim SN, Rusling JF, Papadimitrakopoulos F (2007) Carbon nanotubes for electronic and electrochemical detection of biomolecules. Adv Mater 19:3214–3228
119. Avouris P, Freitag M, Perebeinos V (2008) Carbon-nanotube photonics and optoelectronics. Nat Photon 2:341–350
120. Kivistö S et al (2009) Carbon nanotube films for ultrafast broadband technology. Opt Express 17:2358
121. Rotermund F et al (2012) Mode-locking of solid-state lasers by single-walled carbon-nanotube based saturable absorbers. Quantum Electron 42:663–670
122. Xiao L et al (2008) Flexible, stretchable, transparent carbon nanotube thin film loudspeakers. Nano Lett 8:4539–4545

123. Niu Z et al (2011) Compact-designed supercapacitors using free-standing single-walled carbon nanotube films. Energy Environ Sci 4:1440
124. Niu Z et al (2013) Highly stretchable, integrated supercapacitors based on single-walled carbon nanotube films with continuous reticulate architecture. Adv Mater 25:1058–1064
125. Liu C, Li F, Ma LP, Cheng HM (2010) Advanced materials for energy storage. Adv Mater 22:E28
126. Mustonen K et al (2012) Influence of the diameter of single-walled carbon nanotube bundles on the optoelectronic performance of dry-deposited thin films. Beilstein J Nanotechnol 3:692–702